Naïve Tsunami Generation via Shallow Water Theory

MATH484 Final Project Report

Lonny Cox-Lauf, Jonah Kopp, Clay Kramp, John Luke Lusty

May 8th 2018

"The Great Wave off Kanagawa", Katsushika Hokusai est. 1829

Contents

1 Introduction

A tsunami is a single or series of ocean waves which are generated by sudden displacements in the sea floor, landslides, or volcanic activity [1]. These potentially catastrophic ocean waves frequently occur in a basin of the Pacfic Ocean known as the "Ring of Fire" for its historically intense volcanic activity [1]. Further background into the geological mechanisms resposible for tsunamis can be found in Zirker's (2013) introductory text *The Science of Ocean Waves: Ripples, Tsunamis, and Stormy Seas* [1]. An example of tsunami generation can be seen in figure 1, which was taken from chapter 3 of Marghany's (2018) *Advanced Geoscience Remote Sensing* [2].

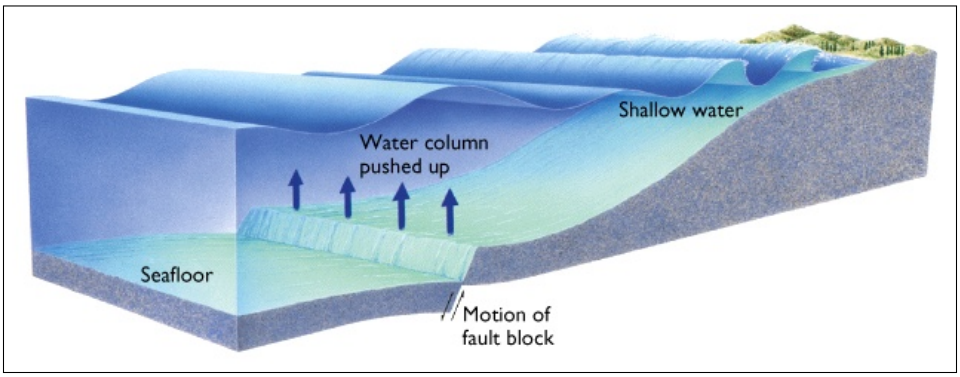

Figure 1: Tsnumai generation due to horizontal seafloor displacement [2].

Transient horizontal displacements resulting from submarine earthquakes and their role in tsunami generation were the focus of Tanioka' and Satake's (1996) study *Tsunami generation by horizontal displacement of ocean bottom* published in Geophysical Research Letters [3]. In this study, they utilize the Satake's (1995) earlier work *Linear and nonlinear computations of the 1992 Nicaragua earthquake tsunami*, which compared and contrasted the success of linear and nonlinear models that governed the generation and propagaion of tsunamis. The linear model utilized in Satake's case study of the Nicaragua earthquake, known as the *shallow-water equations*, and its numerical simulation via a finite-difference method will be the focus of this project.

2 Shallow-Water Theory

Shallow-Water Theory is the canonical mathematical model for waves propagating non-dispersively in a medium which is much wider than it is deep. The *shallow-water equations* are a system of linear partial-differential equations at the center of Shallow-Water Theory. The linear shallow-water equations for a single spatial dimension x and seafloor shape $H = H(x, y)$ are

$$\frac{\partial^2 \eta}{\partial t^2} = \frac{\partial}{\partial x}\left(gH\frac{\partial \eta}{\partial x}\right) + \frac{\partial}{\partial y}\left(gH\frac{\partial \eta}{\partial y}\right). \tag{1}$$

3 The Conservative Form of a Hyperbolic Equation

3.1 Introduction

Before we discuss our process of selection for the scheme used to numerically solve the linear shallow-water equations, it is important to understand the idea of a *conservative form* of a hyperbolic partial-differential equation. First we state the conservative form:

$$\frac{\partial u}{\partial t} + \nabla \cdot \vec{F}(u) = 0, \tag{2}$$

where u is the *density of the conserved quantity*, and $\vec{F}(u)$ is the *density flux*. Note that the actual form of $\vec{F}(u)$ is dependent on the original hyperbolic equation that has been converted into this form. Since u is a density, we will denote its corresponding quantity $\mathbf{u}$ defined by:

$$\mathbf{u} = \int_V u \, dV, \tag{3}$$

where V denotes the spatial domain. In physics, a *conservation law* requires that some measurable property of a system does not change with respect to time. For example, the conservation of mass (ignoring energy) requires that any system with perfectly balanced mass transfers, or net-zero mass flux along its boundaries, cannot change its total mass over time. To illustrate the connection between such a conservation law and the conservative form of a hyperbolic equation, we present a short derivation proving the conservation of the quantity $\mathbf{u}$. To start, integrate both sides of the conservative form 2 term-by-term over the spatial domain V:

$$\int_V \frac{\partial u}{\partial t} dV + \int_V \nabla \cdot \vec{F}(u) \, dV = 0. \tag{4}$$

Now, we apply Leibniz's rule to change the order of differentiation in the first integral:

$$\int_V \frac{\partial u}{\partial t} dV = \frac{d}{dt} \int_V u \, dV. \tag{5}$$

Then, we use the divergence theorem on the second integral, which states that integrating the divergence of the vector field, $\nabla \cdot \vec{F}(u)$, over the spatial domain V is equal to integrating the vector field over the spatial domain's boundary A:

$$\int_V \nabla \cdot F(u) \, dV = \int_A \vec{F}(u) \cdot \vec{n} \, dA, \tag{6}$$

where $\vec{n}$ is the outward-pointing unit vector along the boundary A (see figure 2). By substituting 5 and 6 into 4, one obtains

$$\frac{d}{dt} \int_V u \, dV = - \int_A \vec{F}(u) \cdot \vec{n} \, dA. \tag{7}$$

Thus, the time derivative of **u** (see 3) in V is equal to the net flux across the boundary A (the second integral). Note that the unit vectors $\vec{n}$ are outward-pointing along A, meaning that $-\vec{n}$ must be inward-pointing. Thus, this equation does not necessarily say that **m** is conserved: it is a more general statement that **m** can only change if there is non-zero net flux along the boundary A.

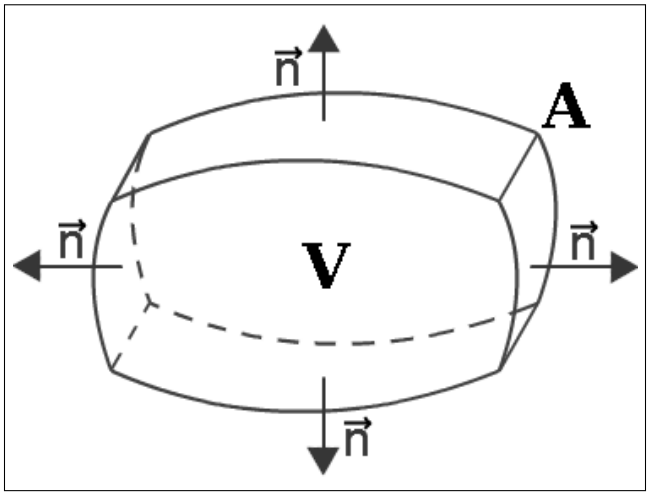

Figure 2: A spatial domain Ω and the unit vectors $\vec{n}$ along its boundary $\partial\Omega$.

Now we return to the law of conservation of mass to provide practical intuition regarding 7. Assume that the physical system in question is a mass distribution m over some spatial domain V, and some mass transfer $\vec{F}(m)$ within V as well as along A. We may state the law of conservation of mass in this case using our previous result 7:

$$\frac{d}{dt}\int_V m\,dV = -\int_A \vec{F}(m)\cdot\vec{n}\,dA. \tag{8}$$

This offers a clearer picture of the significance of the conserved quantity, as in this case it is the total mass **m** of the system:

$$\mathbf{m} = \int_V m\,dV,$$

In the case where the system is isolated with respect to mass transfers, we know that the flux A is zero everywhere along the boundary:

$$\vec{F}(m) = 0, \quad \text{along } A.$$

This implies that

$$\int_A \vec{F}(m)\cdot\vec{n}\,dA = 0, \quad \text{as } \vec{F}(m) = 0 \text{ along } A.$$

Thus, by the statement 8, we have

$$\frac{d}{dt}\int_V m\, dV = \frac{d}{dt}\mathbf{m} = 0,$$

that is: the total mass of our system does not change with respect to time. If a system cannot gain or lose mass, the total mass does not change. However, our statement of 8 allows for a more general result: if the net flux along the boundary is zero, we have:

$$\int_A \vec{F}(m)\cdot\vec{n}\, dA = 0.$$

This implies by 8 that the total mass, yet again, cannot change in time. If a system is given some mass but the exactly same amount of mass is removed from the system, the total mass does not change even though the system is not closed with respect to mass transfers along its boundary. Further, if we know the net flux, then we know exactly how the total mass $\mathbf{m}$ will change in time.

3.2 The Conservative Form of The Shallow-Water Equations

First we derive the conservative form of the 1D Shallow-Water Equations. The 1D form of the equation:

$$\frac{\partial^2 u}{\partial t^2} = \frac{\partial}{\partial x}\left(gH\frac{\partial u}{\partial x}\right) \tag{9}$$

We convert to flux-conservative form by defining two substitution variables:

$$\left.\begin{aligned}\alpha &= \frac{\partial u}{\partial x}\\ \gamma &= \frac{\partial u}{\partial t}\end{aligned}\right\} \Rightarrow \mathbf{U} = \begin{bmatrix}\alpha\\ \gamma\end{bmatrix}.$$

Our goal is to decouple the equation 9 into a system of two equations. This is accomplished by taking derivatives of the above defined substitution variables with respect to time, and applying the law of the equivalence of mixed partials:

$$\begin{aligned}\frac{\partial\alpha}{\partial t} &= \frac{\partial}{\partial t}\frac{\partial u}{\partial x} = \frac{\partial}{\partial x}\frac{\partial u}{\partial t} = \frac{\partial\gamma}{\partial x},\\ \frac{\partial\gamma}{\partial t} &= \frac{\partial}{\partial t}\frac{\partial\gamma}{\partial t} = \frac{\partial^2 u}{\partial t^2} = \frac{\partial}{\partial x}\left(gH\alpha\right).\end{aligned}$$

This leaves us with the system:

$$\frac{\partial}{\partial t}\begin{bmatrix}\alpha\\ \gamma\end{bmatrix} + \begin{bmatrix}\partial_x & 0\\ 0 & \partial_x\end{bmatrix}\left(\begin{bmatrix}0 & -1\\ -gH & 0\end{bmatrix}\begin{bmatrix}\alpha\\ \gamma\end{bmatrix}\right) = \mathbf{0},$$

which is written succinctly as:

$$\frac{\partial\mathbf{U}}{\partial t} + \nabla\cdot\mathbf{F}(\mathbf{U}) = \mathbf{0}.$$

4 Numerical Methodolgy

4.1 A Test Problem

In this section we derive and evaluate a number of common numerical schemes for the solution of a test problem: the wave equation in one dimensions

$$\frac{\partial^2 u}{\partial t^2} = c^2 \frac{\partial^2 u}{\partial x^2} \qquad \text{for } (x) \in V, \tag{10}$$

where c denotes the propagation speed, and V denotes the interior of our spatial domain. For this equation, we consider homogenous Dirchlet boundary conditions

$$u(t, x) = 0 \qquad \text{for } x \in A,$$

where A denotes the exterior of our spatial domain. Finally, we also consider some initial condition

$$u(t, x) = f(x) \qquad \text{for } t = t_0.$$

The equation 1 that we plan to numerically solve is very similar to this equation, as both are linear second-order hyperbolic partial differential equations. Further, we will be using the same boundary and initial conditions. Now, given homogeneous Dirchlet boundary conditions and a gaussian initial condition:

$$f(x) = e^{-x^2},$$

we know that the exact solution is given by:

$$u(t, x) = \frac{1}{2} e^{-(x+ct/2)^2} + \frac{1}{2} e^{-(x-ct/2)^2}.$$

This can be shown using a variety of techniques to solve PDEs, including the Fourier transform. Thus, the initial condition splits into two waves that propagate in opposite directions along the spatial dimension x.

4.1.1 Conservative Form of Test Problem

Here, we state our test problem in conservative form. To do this we define variables γ and α such that:

$$\left.\begin{aligned} \alpha &= c\frac{\partial u}{\partial x} \\ \gamma &= \frac{\partial u}{\partial t} \end{aligned}\right\} \Rightarrow \mathbf{U} = \begin{bmatrix} \alpha \\ \gamma \end{bmatrix}.$$

Now, we take derivatives with respect to time obtain a coupled system of equations:

$$\frac{\partial \alpha}{\partial t} = c\frac{\partial^2 u}{\partial t \partial x} = c\frac{\partial^2 u}{\partial x \partial t} = c\frac{\partial \gamma}{\partial x},$$
$$\frac{\partial \gamma}{\partial t} = \frac{\partial^2 u}{\partial t^2} = c\frac{\partial}{\partial x}\left(c\frac{\partial u}{\partial x}\right) = c\frac{\partial \alpha}{\partial x}.$$

We may write this in matrix form by:

$$\frac{\partial}{\partial t}\begin{bmatrix}\alpha \\ \gamma\end{bmatrix} + \begin{bmatrix}\partial_x & 0 \\ 0 & \partial_x\end{bmatrix}\left(\begin{bmatrix}0 & -c \\ -c & 0\end{bmatrix}\begin{bmatrix}\alpha \\ \gamma\end{bmatrix}\right) = \mathbf{0}.$$

Finally, we note that the numerical scheme will need the initial condition $\mathbf{U}(t=0)$. This is obtained by taking $\alpha(t=0) = f'(x)$ and $\gamma(0) = 0$.

4.2 The Lax-Wendroff Scheme

The Lax-Wendroff scheme [5] is a combination of the Lax-Friedrichs scheme and the leapfrog scheme. Assume that the hyperbolic PDE of interest has been stated in the conservative form:

$$\frac{\partial \mathbf{U}}{\partial t} + \nabla \cdot \mathbf{F}(\mathbf{U}) = 0.$$

The first step is to compute two half-steps, from Lax-Friedrichs:

$$\mathbf{U}_{j+1/2}^{n+1/2} = \frac{1}{2}(\mathbf{U}_{j+1}^n + \mathbf{U}_j^n) - \frac{\Delta t}{2\Delta x}(\mathbf{F}_{j+1}^n - \mathbf{F}_j^n),$$
$$\mathbf{U}_{j-1/2}^{n+1/2} = \frac{1}{2}(\mathbf{U}_j^n + \mathbf{U}_{j-1}^n) - \frac{\Delta t}{2\Delta x}(\mathbf{F}_j^n - \mathbf{F}_{j-1}^n).$$

Now, the flux density $\mathbf{F}$ is evaluated at these half-steps:

$$\mathbf{F}_{j\pm 1/2}^{n+1/2} = \mathbf{F}\left(\mathbf{U}_{j\pm 1/2}^{n+1/2}\right).$$

These are then used in the computation of a leapfrog half-step:

$$\mathbf{U}_j^{n+1} = \mathbf{U}_j^n - \mathbf{F}\left(\mathbf{U}_{j+1/2}^{n+1/2} - \mathbf{U}_{j-1/2}^{n+1/2}\right).$$

A stencil is given from Rezolla [5] illustrating this process in figure 3.

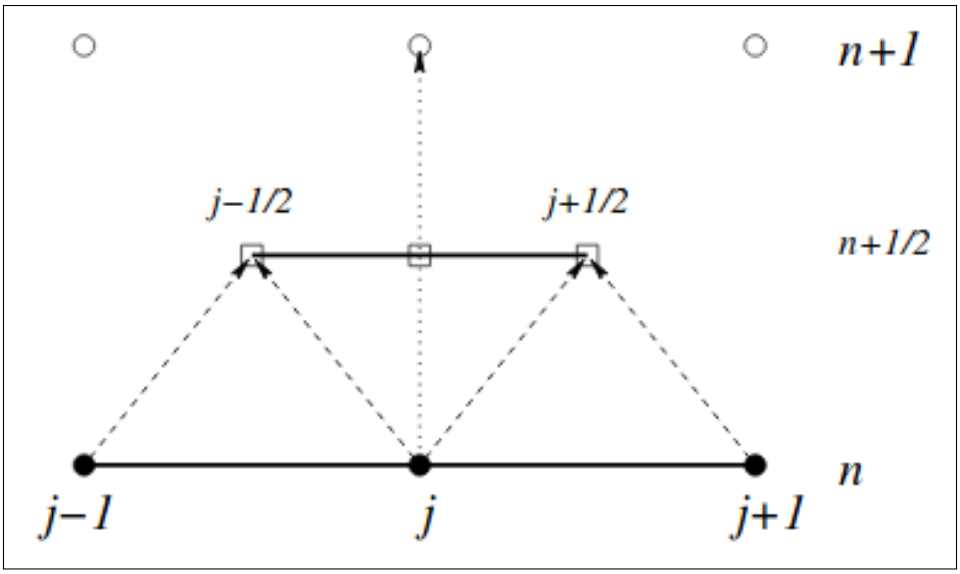

Figure 3: Stencil of the Lax-Wendroff Scheme

4.3 Stability of Lax-Wendroff

In order for Lax-Wendroff to be a stable scheme, the time and spatial discretizations must exactly meet the *Courant-Freidrichs-Löwry condition* [5]:

$$\frac{|v_{\max}|\Delta t}{\Delta x} = 1,$$

where $v_{\max}$ is the maximum velocity of the wave. In practice, this is used to determine the timestep of our method given a spatial discretization:

$$\Delta t = \frac{\Delta x}{|v_{\max}|}.$$

This choice ensures that the propagation speed of the wave is always smaller than the numerical speed of the wave $\Delta x/\Delta t$ [5].

4.4 Boundary Conditions

Our first implementation of Lax-Wendroff applied to the wave equation implemented Dirichlet boundary conditions, with the solution at the endpoints being set to 0. This caused numerical instability in the solution which worsened as the number of time steps used in the discretization increased. Our solution to this was to implement Sommerfeld boundary conditions (also called radiative boundary conditions). These boundary conditions allow the wave to freely move out of our system when it reaches the boundary by applying a numerical scheme for basic advection [5]. The following numerical scheme was implemented to allow the waves to advect from the system:

$$\mathbf{U}_{j+1}^{n+1} = \mathbf{U}_{j}^{n} - \mathbf{U}_{j}^{n+1}Q + \mathbf{U}_{j+1}^{n}Q,$$

for the outer (positive x) edge and

$$\mathbf{U}_{j}^{n+1} = \mathbf{U}_{j+1}^{n} - \mathbf{U}_{j+1}^{n+1}Q + \mathbf{U}_{j}^{n}Q,$$

for the inner (negative x) edge, where

$$Q = \frac{(1-\alpha)}{(1+\alpha)}, \quad \alpha = \frac{|v|\Delta t}{\Delta x},$$

where $|v|$ is the speed of the incident wave to the edge.

4.5 Test Problem Results

Our results match the predicted behavior of the exacted solution.

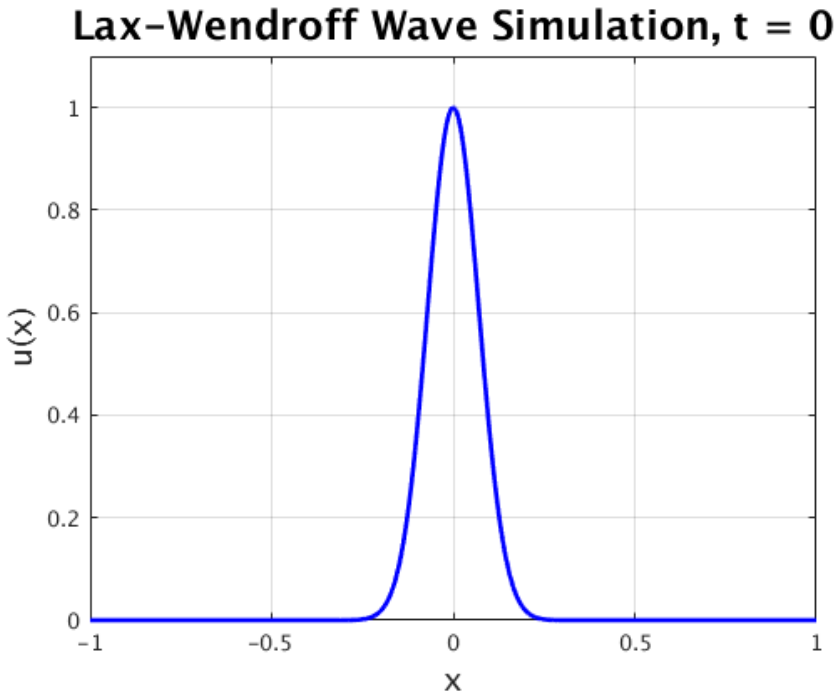

Figure 4: Initial state of the system.

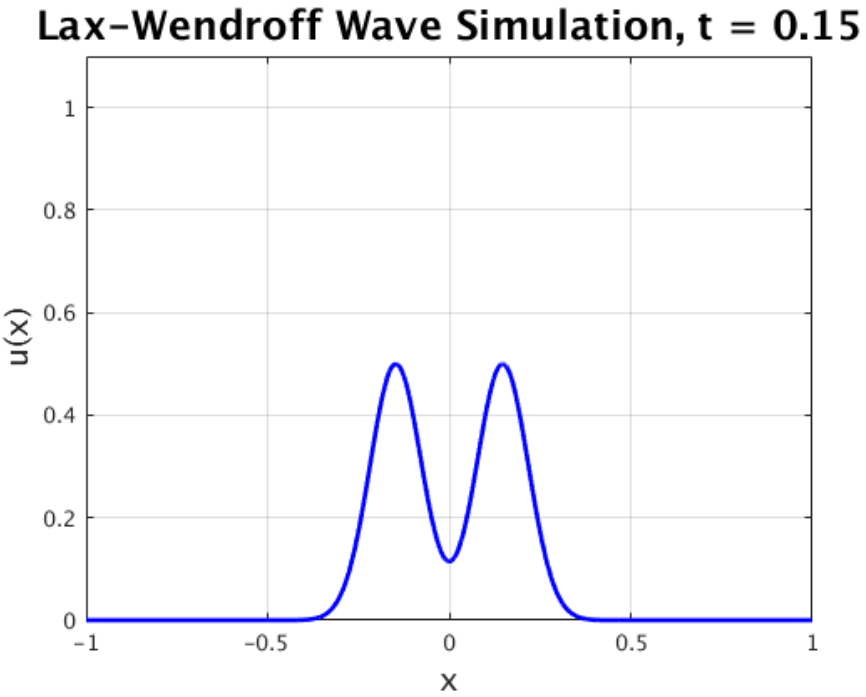

Figure 5: The initial condition beginning to split.

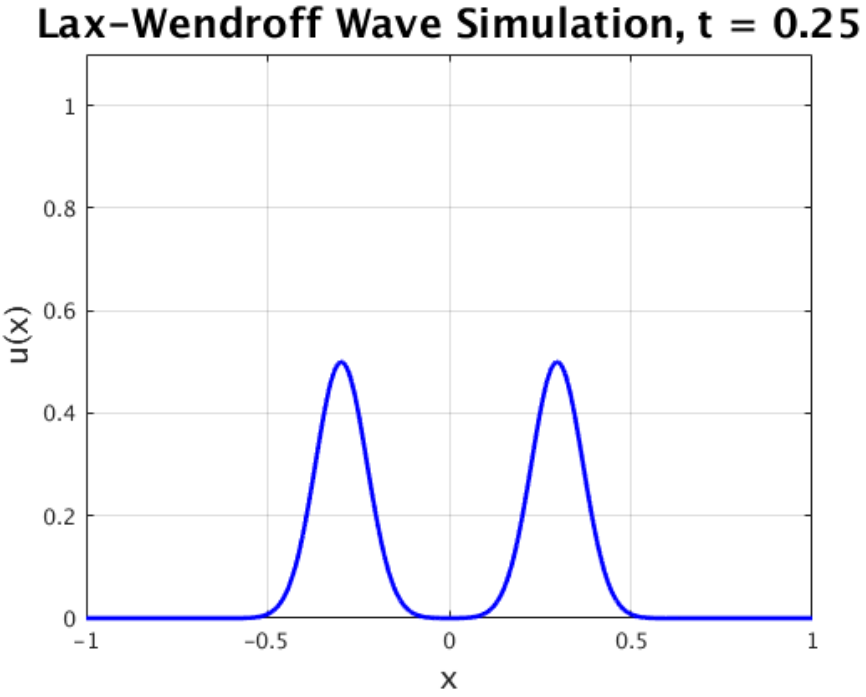

Figure 6: Full split, waves propagating away from origin.

5 Application: Fukushima Daiichi Nuclear Disaster

The shallow water equation requires a choice of a particular seafloor shape $H = H(x, y)$. To test the shallow-water equation, the geography of eastern Japan, specifically Ōkuma, Fukushima will be used and a tsunami resulting from an earthquake with its epicenter at the same location as the Tōhoku earthquake will be simulated. If the tsnumai's wave front reaches the Fukushima Daiichi Nuclear Power Plant, it will be demonstrated whether or not the shallow-wave equation is suitable for simulating not only tsunamis, but areas that may be at risk of flooding from tsunamis.

6 Interpolating Sea Floor: Fukushima Daiichi Nuclear Disaster

A Bézier curve is a parametric curve used to model smooth curves. In order to develop the sea floor map (without having to define every single point), we decided to use a cubic Bézier Curve. A cubic Bézier curve takes in 4 control points and interpolates along the 4 points to develop a smooth, continuous curve. The control points are defined as two points at the ends, one at $\frac{1}{3}$ of the way, and another at $\frac{2}{3}$ of the way. Now, provided the control points, we have the following explicit form:

$$B(t) = (1-t)^3 P_0 + 3t(1-t)^2 P_1 + 3t^2(1-t)P_2 + t^3 P_3, \quad 0 \le t \le 1 \tag{11}$$

Where P is the control point. We can use this explicit form to find the derivative at any point t:

$$B'(t) = 3(1-t)^2(P_1 - P_0) + 6t(1-t)(P_2 - P_1) + 3t^2(P_3 - P_2), \quad 0 \le t \le 1 \tag{12}$$

We can extend the idea of a Bézier curve to develop a Bézier surface, which is a 2D linearly interpolated surface that is made using 16 control points. The 16 control points create a 4×4 grid of points. In order to find a single point on the surface, say (u, v), we first create 4 new points by evaluating (11) at u using 4 sets of 4 control points. That is, we calculate $B(u)$ using control points 1 through 4, then 5 through 8, 9 through 12, and finally 13 through 16. We then use the 4 values of $B(u)$ as control points, and evaluate $B(v)$ to finally find the point on surface (u, v). This method is repeated on all points on the grid, in order to create the Bézier surface.

6.1 Implementation

For our application with the Fukushima Daiichi Nuclear Power Plant, we derived the 4 control points for the sea floor using the National Oceanic and Atmospheric Administration's (NOAA) Bathymetric Data Viewer. The viewer allows users to gain elevation data at any coordinate. Thus, we drew a line between the epicenter of the earthquake to the nuclear power plant, and derived the 4 control points from there.

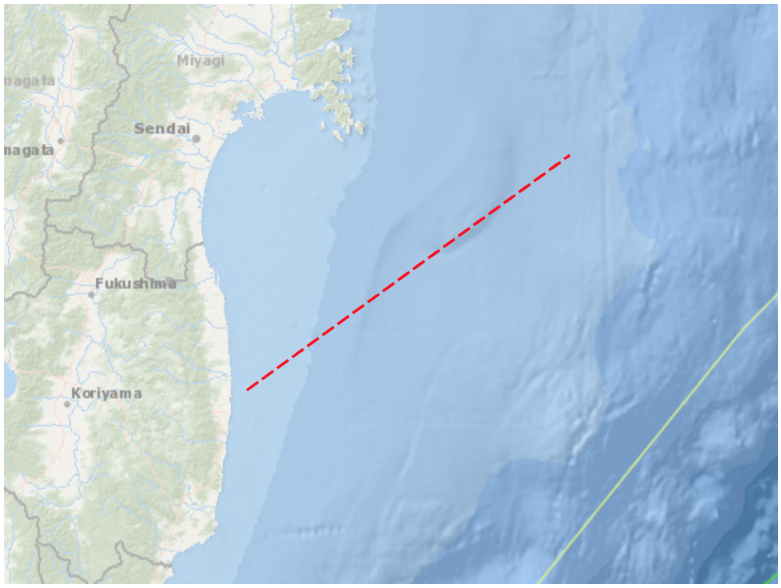

Using the control points, we can then apply the cubic Bézier curve to derive the following sea floor curve:

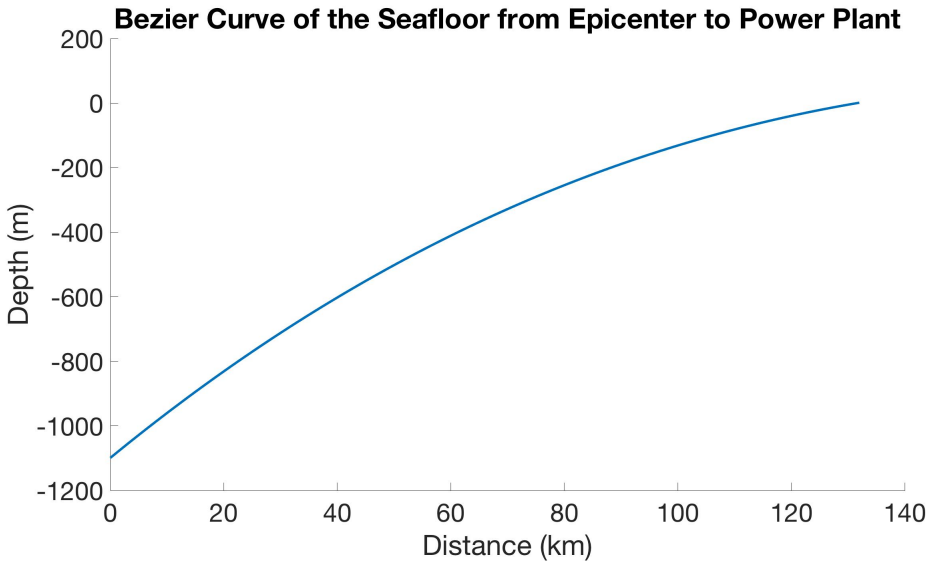

Similarly, we can also draw a rectangle with the diagonal being the line between the epicenter of the earthquake to the nuclear power plant. This rectangle is then used to define the 16 control points in order to derive the 2D interpolated sea floor surface.

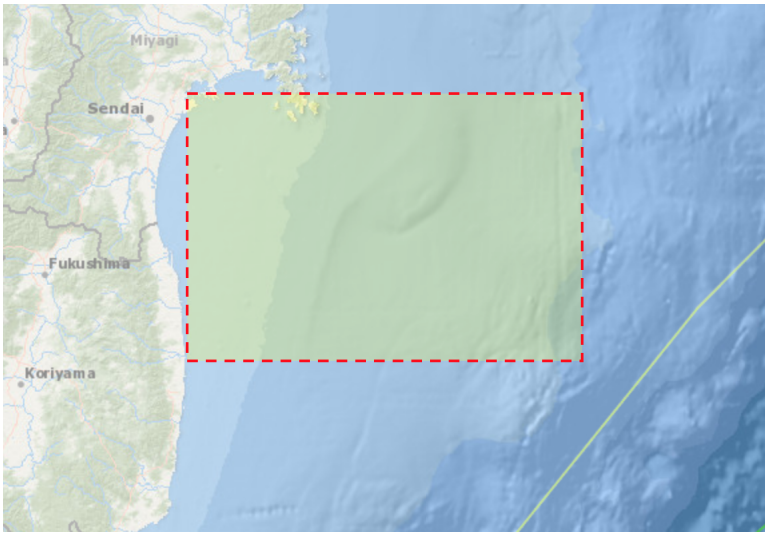

Using the control points, we linearly interpolate all the points within the grid, and derive the following sea floor.

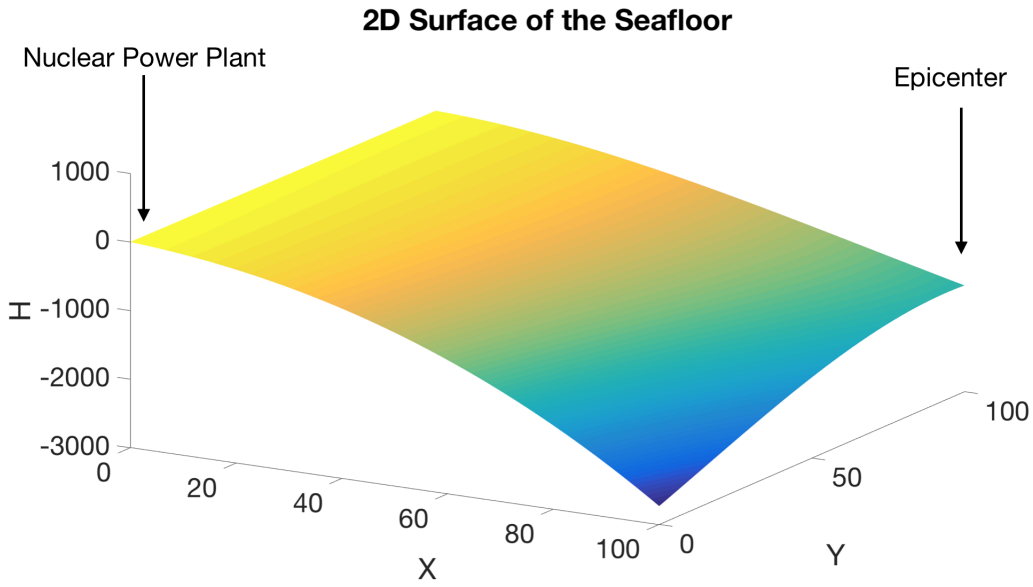

The key benefit of using the Bézier cubic interpolation is that we can create approximations of the sea floor very easily with only a few defined points. This gives us the liberty to apply our numerical method to any geographical location, and even test it with fictional surfaces.

Using Equation 12 for the derivative at any point t, we now generate three-dimensional surface plots describing the partial derivatives with respect to x and y of the Bezier surface. These derivatives for x and y are stored in two matrices, each of size 100x100, where the i,

j element of each represents the partial derivative at x location, i, and y location, j. The images below are useful visual representations of these derivatives.

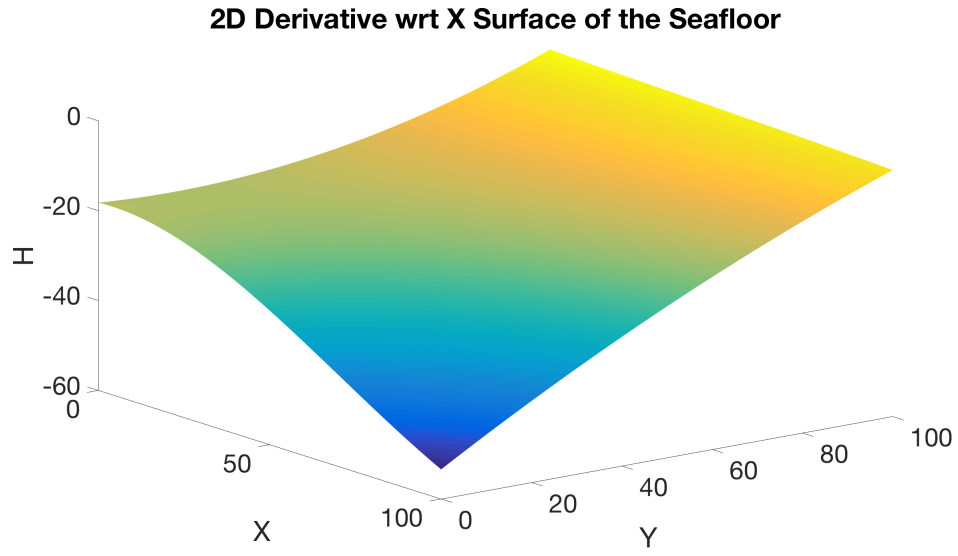

Figure 7: This is a surface plot of the derivative at each grid point with respect to x

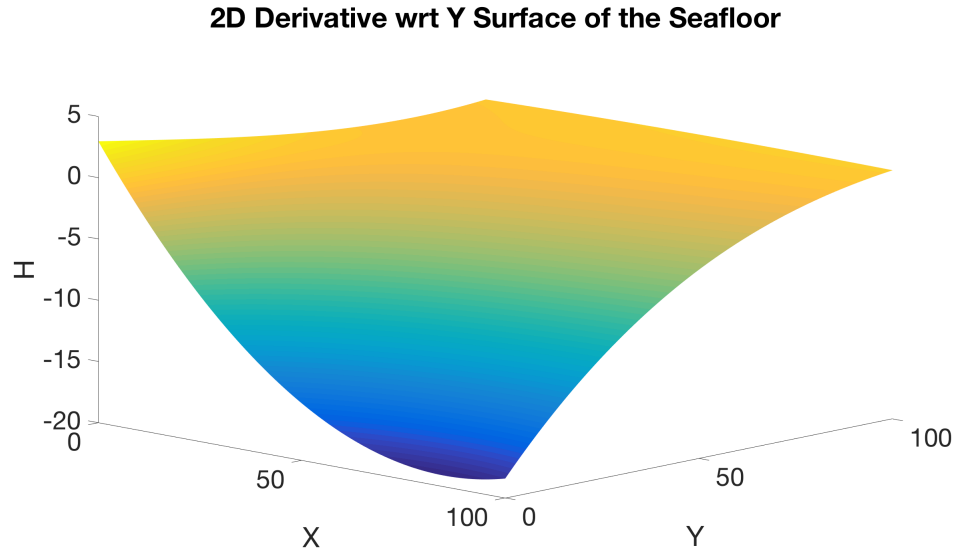

Figure 8: This is a surface plot of the derivative at each grid point with respect to y

These derivatives at each grid point are necessary for stepping forward in our model in order to better simulate the dynamics of the wave. This allows us to estimate the amplitude of the wave once reaching the nuclear power plant, which is assumed to be located a neglibible distance from the coast at which the elevation is set to the value 1 meter.

7 Results

We implemented the tsunami simulation for the 1D case. We use the surface developed previously to simulate the tsunami given an initial perturbation.

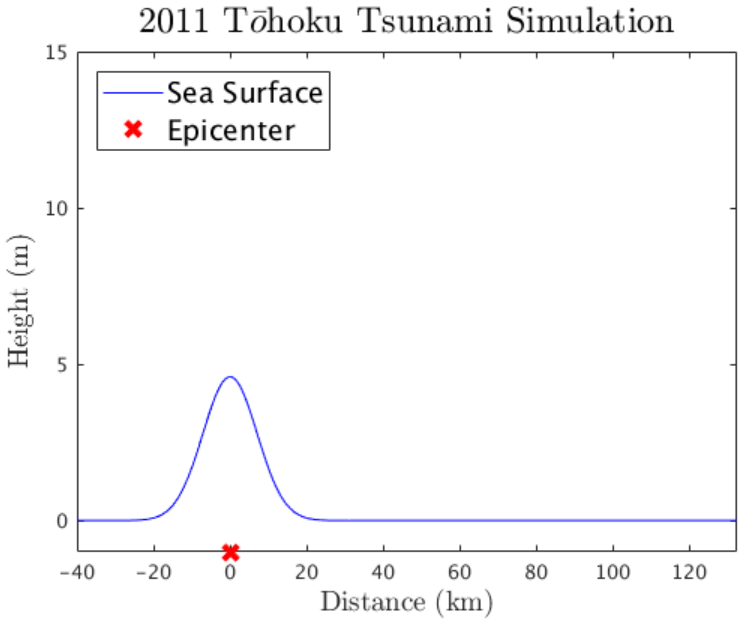

When the simulation begins, we see the perturbation split into two separate waves, one that travels to the power plant and one that travels away.

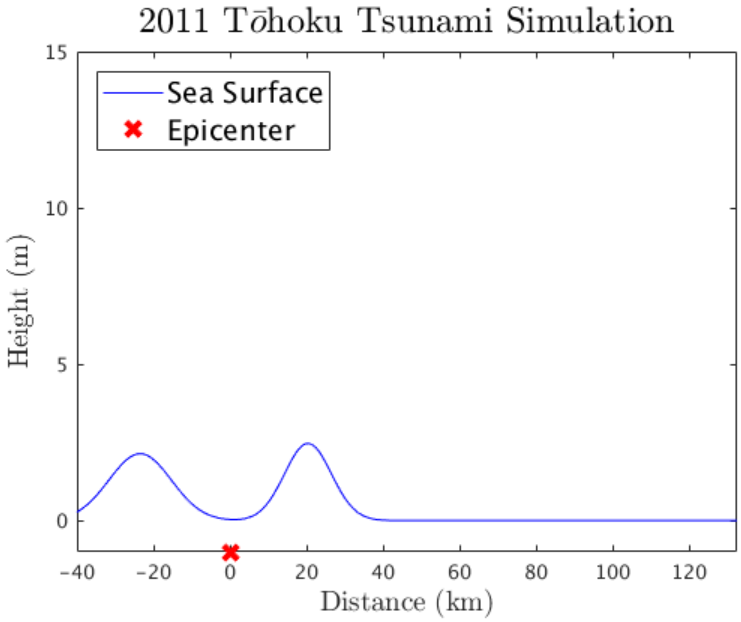

As the tsunami approaches the power plant, we examine the change in the wave's height. Reports indicate that the actual tsunami in 2011 reached a height of 15 meters by the time it reached the power plant site [6]. In our simulation, we see that when the tsunami's right edge comes in contact with the coast, the tsunami's amplitude reaches 15 meters.

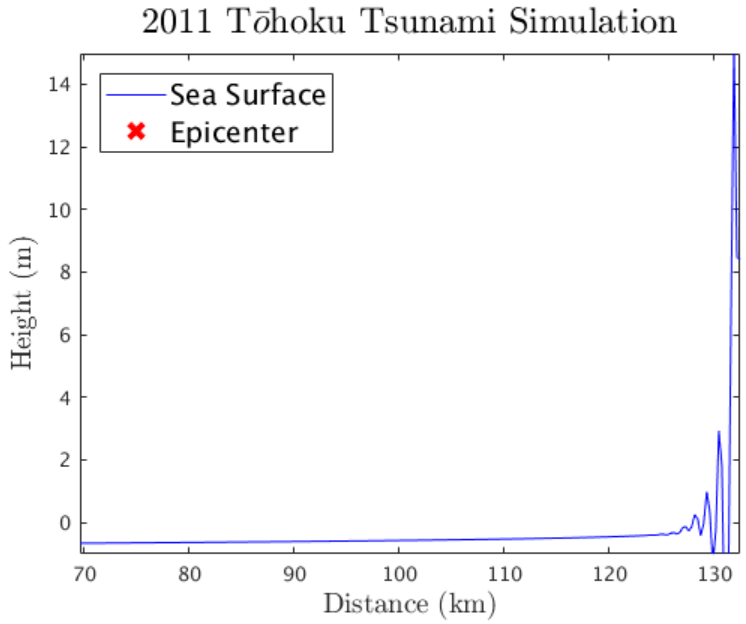

Figure 9: The simulated tsunami breaches the shore.

The simulation also reflects the effects of wave shoaling. Wave shoaling is an effect that occurs when a wave moves from a deep to shallow region. Shoaling causes waves to slow, decrease in wavelength, and magnify in amplitude [1]. This occurs in order to maintain constant energy flux within the wave. This effect is particularly pronounced at the coast, where the seafloor approaches sea level. In the simulation, we see that the wave's amplitude rapidly increases as it reaches the coast, which is a direct reflection of wave shoaling. We also see that shoaling affects the wave traveling away from the power plant as well. As the seafloor continues to decrease, we see the wave flatten out and increase in speed.

We also see that in the final frame, there is visible numerical dispersion behind the wavefront. This is due to our numerical solver, Lax-Wendroff's uses Lax-Friedrich's, which has the Courant-Friedrichs-Löwy condition:

$$1 = \frac{|v|\Delta t}{\Delta x}$$

.

However, in our implementation, the value $|v|$ is computed at the initial time step using current velocity data. As we have shown previously, velocity changes with time due to shoaling, and the CFL condition is no longer met by our final time step. This leads to numerical dispersion, as can be seen in 9. In future work, we would like to use an adaptive

method so that the CFL condition is always met. This will control the numerical dispersion and lead to a more accurate model.

8 Conclusion

The shallow-water wave equation provides a strong starting point for analyzing the propagation and growth of waves over a known sea floor (or any surface supporting a body of water). However, in order to achieve this desired result we had to make several assumptions. The perturbation that we use to represent the initial state of the tsunami is not representative of nature. In nature, we would expect a pressure wave emanating radially from the epicenter to propagate evenly in all directions. This would lead to a much shorter initial wave (which may still be Gaussian, just with a larger sigma parameter), and the water beneath the surface wave would also have behavior significant to the generation of the tsunami. Essentially, a more accurate model would account for a pressure wave beginning at the epicenter and expanding evenly in all directions, showing more behavior than just at the surface.

Despite the limitations of the model as-is, we achieved our goal of numerically solving the shallow-water wave equation in one dimension given the shape of the sea floor below. We were also able to apply a new sort of boundary condition, a radiation condition, which allowed the wave to leave the system without reflecting back in. This worked much better than our initial attempt of using Dirichlet boundary conditions, setting the height of the wave to 0. This first attempt introduced significant numerical instability.

Going forward, we would like to see our method implemented in 2D. We finished creating the smooth 2D sea floor and finding the x and y derivatives, but did not implement the Lax-Wendroff numerical scheme in 2D. Additionally, we would like to take steps to make this simulation closer to what would be observed in nature–perhaps starting the simulation before the earthquake occurs, having a model that can handle a rapid shift of the sea floor. An integral formulation of the equation may be able to handle such discontinuities.

Our naïve approach to the generation of tsunamis may not have been exactly representative of nature, but the growing height of the wave as it approached the shore is an accurate representation of how the sea floor affects approaching waves. Adjusting the parameters and initial perturbation may facilitate more accurate simulations, allowing for rough approximations to tsunamis all over the world, provided the sea floor elevation data is readily available.

References

[1] Jack B Zirker. *The Science of Ocean Waves: Ripples, Tsunamis, and Stormy Seas*. John Hopkins University Press, 22 October 2013. Accessed via Arthur Lakes Library at the Colorado School of Mines, March 31, 2018.

[2] Maged Marghany. *Simulation of Tsunami Impact on Sea Surface Salinity along Banda Aceh Coastal Waters, Indonesia*. Advanced Geoscience Remote Sensing, Ch 3. Intech, 2014. Accessed via In Tech Open, March 31, 2018.

[3] Yuichiro Tanioka, Kenji Satake. *Tsunami generation by horizontal displacement of ocean bottom*. Geophysical Research Letters, Vol 3, No 8, 15 April 1996. American Geophysical Union Publications. Accessed via Wiley Online Library, March 31, 2018.

[4] Rick Salmon. *Introduction to Ocean Waves*. Scripps Institution of Oceanography, University of California, San Diego, 7 December 2015. Accessed via Rick Salmon's website via http://pordlabs.ucsd.edu/rsalmon/, March 31, 2018.

[5] Luciano Rezzolla. *Lecture Notes on Numerical Methods for the Solution of Hyperbolic Partial Differential Equations*. SISSA, International School of Advanced Studies, Trieste, Italy, 2 August 2015. Accessed via Luciano Rezzolla's website via http://www.sissa.it/ rezzolla, March 31, 2018.

[6] World Nuclear Association. *Fukushima Accident*. October, 2017. Accessed via http://www.world-nuclear.org/information-library/safety-and-security/safety-of-plants/fukushima-accident.aspx, May 3, 2018.